JOURNAL OF GEOPHYSICAL RESEARCH: OCEANS, VOL. 119, 496–508, doi:10.1002/2013JC009346, 2014

Diffusive vertical heat flux in the Canada Basin of the Arctic Ocean inferred from moored instruments

Camille Lique,[1,2] John D. Guthrie,[3] Michael Steele,[3] Andrey Proshutinsky,[4] James H. Morison,[3] and Richard Krishfield[4]

Received 9 August 2013; revised 12 December 2013; accepted 15 December 2013; published 22 January 2014.

[1] Observational studies have shown that an unprecedented warm anomaly has recently affected the temperature of the Atlantic Water (AW) layer lying at intermediate depth in the Arctic Ocean. Using observations from four profiling moorings, deployed in the interior of the Canada Basin between 2003 and 2011, the upward diffusive vertical heat flux from this layer is quantified. Vertical diffusivity is first estimated from a fine-scale parameterization method based on CTD and velocity profiles. Resulting diffusive vertical heat fluxes from the AW are in the range 0.1–0.2 W m^{-2} on average. Although large over the period considered, the variations of the AW temperature maximum yields small variations for the temperature gradient and thus the vertical diffusive heat flux. In most areas, variations in upward diffusive vertical heat flux from the AW have only a limited effect on temperature variations of the overlying layer. However, the presence of eddies might be an effective mechanism to enhance vertical heat transfer, although the small number of eddies sampled by the moorings suggest that this mechanism remains limited and intermittent in space and time. Finally, our results suggest that computing diffusive vertical heat flux with a constant vertical diffusivity of $\sim 2 \times 10^{-6}$ m^2 s^{-1} provides a reasonable estimate of the upward diffusive heat transfer from the AW layer, although this approximation breaks down in the presence of eddies.

Citation: Lique, C., J. D. Guthrie, M. Steele, A. Proshutinsky, J. H. Morison, and R. Krishfield (2014), Diffusive vertical heat flux in the Canada Basin of the Arctic Ocean inferred from moored instruments, *J. Geophys. Res. Oceans*, *119*, 496–508, doi:10.1002/2013JC009346.

1. Introduction

[2] Warm water ($T > 0°C$) originating from the North Atlantic feeds the intermediate layer of the Arctic Ocean. As it circulates cyclonically around the Eurasian and the Canadian Basins, Atlantic Water (AW) carries enough heat to melt all the sea ice in a few years if the heat was brought to the surface [*Turner*, 2010]. However, the transfer of heat from the AW layer to the overlying layers is limited by the strong stratification in the surface and subsurface layers [*Aagaard et al.*, 1981; *Rudels et al.*, 1996; *Toole et al.*, 2010], whose maintenance is enhanced by the low level of mixing in the Arctic interior [*Rainville and Winsor*, 2008; *Fer*, 2009]. From heat budget considerations, comparing the heat carried by the AW at the entrance and the exit of the Arctic Basin, *Turner* [2010] evaluates a required vertical heat flux from the AW layer of 6.7 W m^{-2} to maintain a steady state. As enhanced mixing occurs over steep bathymetry, *Sirevaag and Fer* [2012] reduce this amount to 4 W m^{-2} in the Arctic interior. However, direct estimations of the vertical heat flux in the Arctic Basin remain very sparse both in time and space, and range over several orders of magnitude from less than 1 W m^{-2} in the interior of the Canadian Basin [*Rainville and Winsor*, 2008] to ~25 W m^{-2} over the Yermack Plateau [*Padman and Dillon*, 1991; *D'Asaro and Morison*, 1992] or O(100−150) W m^{-2} north of Svalbard [*Steele and Morison*, 1993; *Fer et al.*, 2010]. More observations are required to better constraint the heat budget for the AW layer, and in particular to better estimate the relative contributions of the quiet interior of the basins, in contrast to the more energetic boundary regions.

[3] On top of this long-term steady state, the AW temperature is also influenced at inflow straits by strong interannual to decadal variability [e.g., *Polyakov et al.*, 2004]. An anomalously warm pulse of AW entering the Arctic through Fram Strait was first detected in the very early 1990s [*Quadfasel et al.*, 1991], and propagated along the Eurasian continental slope, and major ridge systems reaching the North Pole and central basin by 1993 [*Carmack et al.*, 1997; *Morison et al.*, 1998]. With some variability,

[1]Joint Institute for the Study of the Atmosphere and Ocean, University of Washington, Seattle, Washington, USA.
[2]Now at Department of Earth Sciences, University of Oxford, Oxford, UK.
[3]Polar Science Center, Applied Physics Laboratory, University of Washington, Seattle, Washington, USA.
[4]Woods Hole Oceanographic Institution, Woods Hole, Massachusetts, USA.

Corresponding author: C. Lique, Department of Earth Sciences, University of Oxford, South Parks Road, Oxford OX1 3AN, UK. (camille@earth.ox.ac.uk)

2169-9275/14/10.1002/2013JC009346

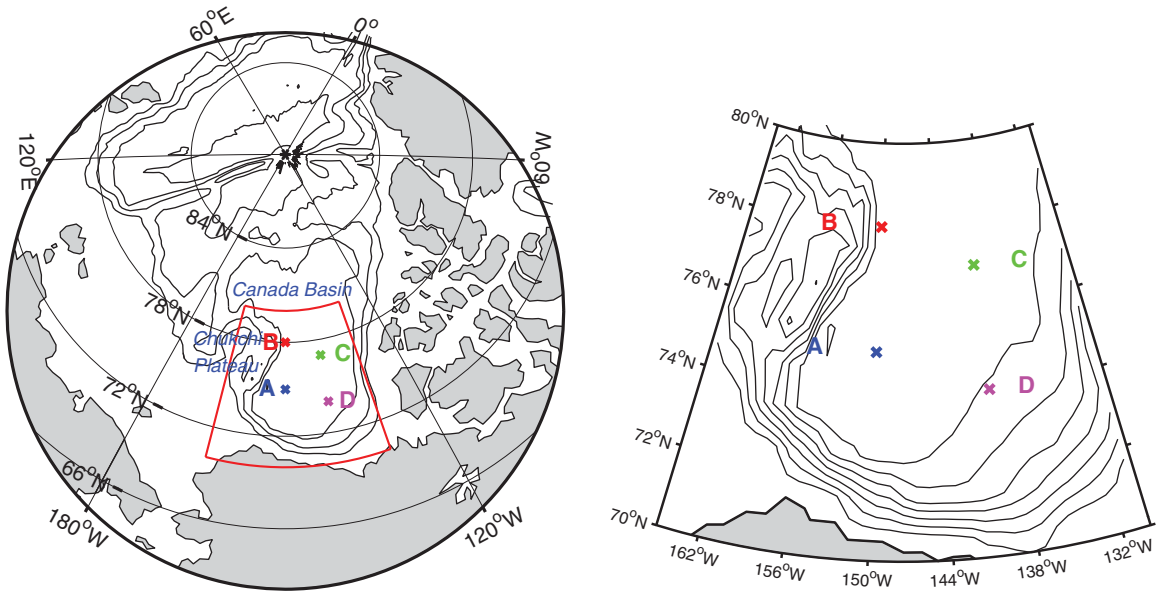

Figure 1. Location of the four BGOS moorings. Bathymetry contours are shown (left) every 1000 m and (right) every 500 m. The red box delimits the region on which a zoom is done.

the temperature anomalies of up to 1°C (relative to measurements in the 1970s and 1980s) have persisted in the 2000s [e.g., *Polyakov et al*., 2004]. The warming also reached the Canada Basin by the mid 1990s [*Carmack et al*., 1995], first along the slope [*Smethie et al*., 2000; *Shimada et al*., 2004], and then reached the interior of the Canada Basin by the 2000s [*McLaughlin et al*., 2009].

[4] Using hydrographic observations supplemented by 1-D and 3-D model results, *Polyakov et al*. [2010] suggest that the AW warming observed in the 2000s in the Eurasian and Makarov Basins, associated with a 75–90 m shoaling of the upper AW boundary, yielded a warming of the overlying cold halocline through an increase of the upward vertical heat flux from the AW layer. In contrast, direct microstructure observations conducted in Spring 2007 in the interior of the Amundsen Basin reveal that the quantity of heat released upward from the AW layer remains really small in this region [*Fer*, 2009].

[5] In the present study, we aim at estimating the diffusive vertical heat flux from the AW layer in the interior of the Canadian Basin and its contribution to the AW heat budget. We also aim at examining the possible consequences of the warming observed in the AW layer of the Canada Basin for the overlying layers. In this region of the Arctic Ocean, the AW temperature maximum is found deeper than in the Eurasian Basin (∼400–500 m), and the surface and subsurface layers are composed of inputs of both Pacific and Atlantic-origin waters, making the vertical structure more complex [*Shimada et al*., 2005]. As the AW is far below surface, any increase of the vertical heat flux is not necessarily going to reach the surface and thus the sea ice. From microstructure measurements in the 1980s, *Padman and Dillon* [1987] conclude that the upward vertical heat flux from AW in the central Canada Basin is very small. This conclusion, however, could be called into question, in light of recent observations reporting an unprecedented warm anomaly of the AW layer in the southern Canada Basin (with an temperature increase of ∼0.25°C) [*McLaughlin et al*., 2009]. The idea is that, although vertical mixing of temperature is small in the Arctic interior [*D'Asaro and Morison*, 1992; *Rainville and Winsor*, 2008], a change of the temperature gradient could lead to significant heat flux variations.

[6] Here, observations from four profiling moorings deployed in the Canada Basin are used to compute the diffusive vertical heat flux from the AW layer and to examine its variations over the period 2003–2011. The remainder of this paper is organized as follows. The mooring observations used for the study are described in section 2. In section 3, we describe the method used to estimate the vertical diffusivities, and to compute the diffusive vertical heat fluxes. Results of the calculations are presented in section 4, and we investigate different mechanisms responsible for the variability of the diffusive vertical heat flux in section 5. Summary and conclusions are given in section 6.

2. Mooring Observations

[7] As part of the Beaufort Gyre Observing System (BGOS, www.whoi.edu/beaufortgyre) [*Proshutinsky et al*., 2009], up to four moorings have been deployed and maintained in the Canada Basin since August 2003 (A, B, C, and D, see Figure 1). Each mooring carries a McLane moored profiler (MMP), which includes a Falmouth Scientific Inc. (FSI) conductivity-temperature-depth (CTD) sensor and a FSI acoustic current meter (ACM) to record current and hydrographic profiles from about 60 to 2000 m. The MMP acquires data at a speed of 25 cm s^{-1} (with 1 Hz sampling rate) along one-way profiles separated in time alternately by 6 and 48 h intervals. We use the processed data interpolated to a 2 m fixed vertical grid, downloaded on 25 June 2012 at http://www.whoi.edu/page.do?pid=66559, covering the period from August 2003 to August 2011. The data processing procedures are described in

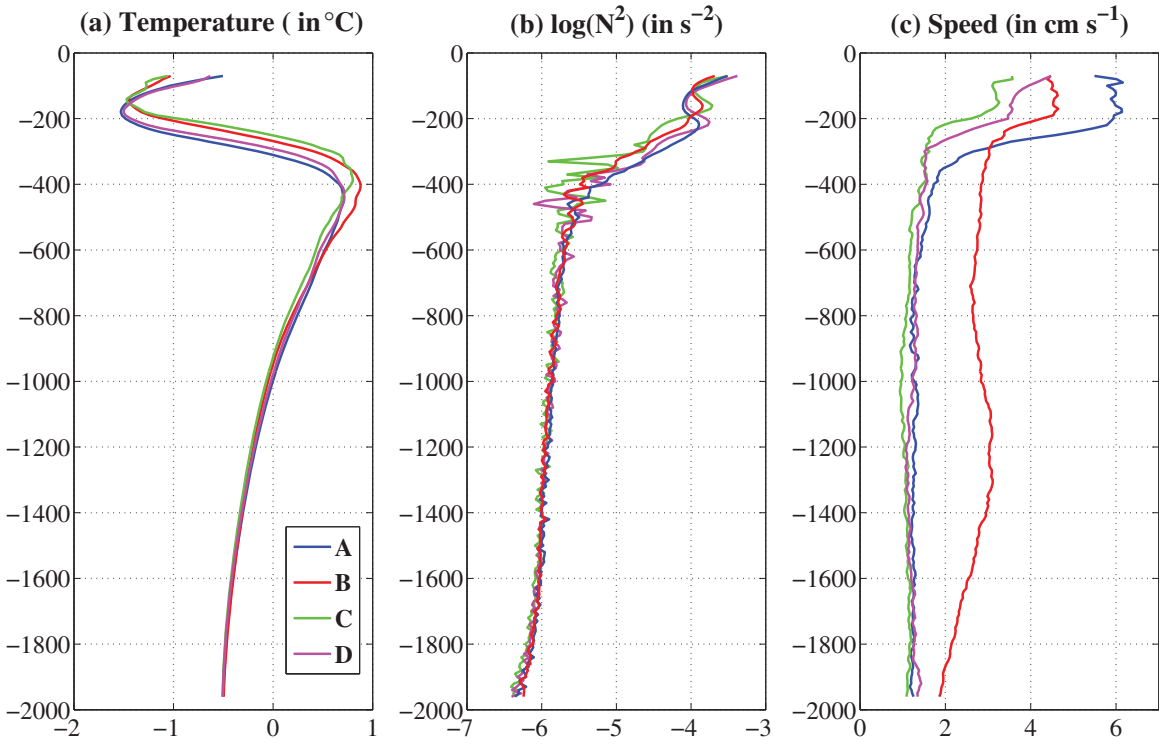

Figure 2. Time averaged profiles of (a) temperature, (b) buoyancy frequency squared (N^2), and (c) speed (defined as $\sqrt{U^2+V^2}$) for the four moorings. All the quantities have been interpolated into a 10 m vertical resolution grid, and the pair of profiles corresponding to the up and down MMP profiles have been averaged together first to produce daily values.

"BGFE 2003–2004 MMP EMCTD and ACM Data Processing Procedures," by R. Krishfield et al. (unpublished technical report, 2013, available at http://www.whoi.edu/fileserver.do?id=85606&pt=2&p=100409). According to the manufacturer, the FSI CTD measures temperature and salinity with the resolution of 0.01°C and 0.02 psu, respectively, and are confirmed by laboratory calibrations or in situ comparison against shipboard CTD data before each deployment. The MMP FSI ACM current velocity precision and resolution are reported by the manufacturer to be 3% of reading and ±0.01 cm s^{-1}, respectively. Compass accuracies are ±2° which are confirmed by spin calibrations on each instrument prior to each deployment.

[8] Mean profiles of temperature, buoyancy frequency, and speed for the four moorings are shown in Figure 2, and Figure 3 shows the time-depth evolution of the temperature and the buoyancy frequency. As the top of the MMPs is located between 50 and 100 m, they sample the water column below the local maximum temperature corresponding to summer pacific water [*Steele et al.*, 2004]. The mean temperature profiles show a minimum around 150–200 m, due to the presence of Pacific Winter Water (PWW) [e.g., *Coachman and Barnes*, 1961], and then a transition toward the AW maximum temperature (~0.8°C at 400 m). Below this depth, the buoyancy frequency becomes small and roughly constant. Although the four moorings exhibit very similar mean temperature and buoyancy frequency profiles, they show different mean speed profiles. Mooring A samples higher speeds, with a maximum around 6 cm s^{-1} versus 3–4 cm s^{-1} at moorings C and D. The difference is due to the presence of short events with very high velocity at mooring A rather than constant higher speed. These events are related to the presence of eddies at this location, which tend to increase the time-average speed profile. Eddies are further described in section 5. The mean velocity from mooring B below 200 m is much larger than from the other moorings. This is due to the presence of numerous deep eddies only captured by mooring B, with velocities around 20 cm s^{-1}, as described in detail by *Carpenter and Timmermans* [2012].

3. Calculation Method

[9] CTD and ACM profiles from the four moorings are used to estimate the vertical heat flux through the sampled water column. Vertical heat flux due to diffusion can be expressed as:

$$F_H = \rho C_p K_Z \frac{\partial T}{\partial z} \tag{1}$$

with T the temperature, K_Z the vertical diffusivity, ρ the density of ocean water, and C_p the ocean specific heat capacity. F_H is positive upward and in the units of W m^{-2}.

[10] Vertical diffusivity requires microstructure measurements to be directly estimated. In the Arctic interior, *Rainville and Winsor* [2008] have measured diffusivities of the order of 10^{-6} m^2 s^{-1}. Owing to their difficulty, these

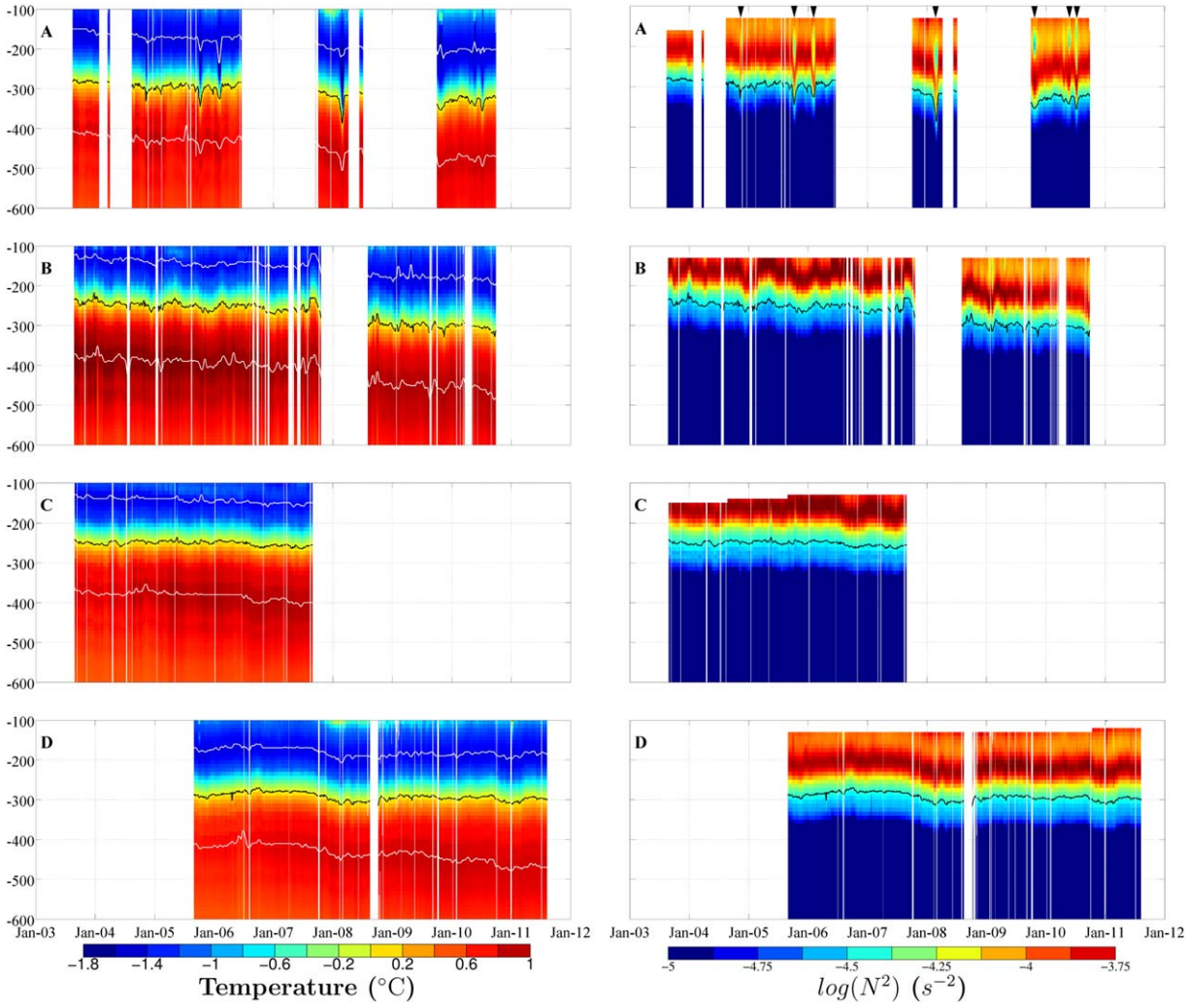

Figure 3. Temperature and buoyancy frequency as a function of time and depth for the moorings A, B, C, and D (from top to bottom). The black line indicates the depth of the 0°C contour for the temperature that represents the limit of the AW temperature. The two white lines indicate the depth of the maximum (lower one) and the minimum (upper one) temperatures. The black arrow on the right top plot indicates the presence of eddies.

kinds of measurements are rare in the Arctic, but less demanding fine-structure velocity measurements can be used to infer Arctic Ocean deep background mixing consistent with internal wave dynamics [*D'Asaro and Morehead*, 1991; *D'Asaro and Morison*, 1992].

[11] Away from the direct influence of the boundary and the topography, most of the ocean mixing is driven by breaking internal gravity waves [*Polzin et al*., 1997]. Here, we will estimate K_Z using a parameterization accounting for energy dissipation by internal waves breaking [*Gregg*, 1989; *Kunze et al*., 2006]. In weak background mixing environments such as the Arctic interior, staircases can be observed in temperature and salinity profiles, suggesting the existence of double diffusion [*Timmermans et al*., 2008b]. However, the studies of *Merryfield* [2000] or *Inoue et al*. [2007] indicate that background mixing and double diffusive mixing are not mutually exclusive. In the present study, we only consider mixing due to internal wave breaking, but the reader should keep in mind that other processes might be of importance for the vertical mixing at some depths and in some regions of the Arctic Ocean, in particular double diffusive mixing [*Padman and Dillon*, 1987, 1988, 1989; *Timmermans et al*., 2008b; *Sirevaag and Fer*, 2012; *Polyakov et al*., 2012].

3.1. Vertical Diffusivity From Fine-Scale Parameterization

[12] Based on the idea that internal waves act to transfer energy from the large vertical scales (at which they are generated and propagate) to the small scales (at which they break), the vertical diffusivity can be expressed as [*Gregg et al*., 2003; *Kunze et al*., 2006]:

$$K_Z = K_{Z0} \frac{<V_z^2>^2}{<V_z^2>_{GM}^2} h_1(R_\omega) L(f, N) \qquad (2)$$

where $<V_z^2>$ is the observed fine-scale shear variance, $<V_z^2>_{GM}$ is the corresponding value estimated from the Garrett-Munk (GM) model spectrum, $K_{Z_0} = 5 \times 10^{-6} m^2 s^{-1}$

is the background mixing level for GM conditions, and the terms h_1 and L are given as:

$$h_1(R_\omega)=\frac{3(R_\omega+1)}{2\sqrt{2}R_\omega\sqrt{R_\omega-1}} \text{ and } L(f,N)=\frac{f\cosh^{-1}(N/f)}{f_{30}\cosh^{-1}(N_0/f_{30})}$$

[13] Here, $L(f, N)$ accounts for the latitudinal variation, N is the local buoyancy frequency, f is the local inertial frequency, N_0 is the reference stratification (equals to 5.2×10^{-3} s^{-1} corresponding to 3 cycles/h), and f_{30} is the inertial frequency at 30° latitude. h_1 corrects for the variations in the shear (the vertical gradient of horizontal velocity due to internal wave propagation, V_z) − strain (the vertical gradient of isopycnal displacement due to internal wave propagation, ξ_z) ratio expressed as:

$$R_\omega=\frac{<V_z^2>}{N^2<\xi_z^2>} \tag{3}$$

[14] Each profile is processed independently. Raw profiles are first visually inspected to discard outliers. The fine-scale parameterization is then applied to each profile. Resulting profiles of vertical diffusivity are again visually inspected and inaccurate values are discarded as described in the following. The very small values for velocities combined with low stratification found in the deeper part of the sampled water column yields high and likely unrealistic values for the vertical diffusivity. For this reason and because we focus mainly on the upper portion of the AW, we limit the results to the part of the water column shallower than the AW temperature maximum.

[15] K_Z is computed over a 10 m resolution grid starting from the first good data point. Following *Fer et al*. [2010] and *Guthrie et al*. [2013], values of shear and strain variance are obtained from moving 128 m (64 point) segment spectral analysis, calculated every 10 m. As the moving window is larger than the grid resolution, the estimations at different levels are not independent. The results show, however, little sensitivity to the choice of these parameters. Window choices of 64, 128, and 256 m did very little to alter profile shape. Shear spectra are computed as total velocity spectra multiplied by $(2\Pi \times k_z)^2$, where k_z is the vertical wave number and then normalized by the mean N^2 for the segment. The spectra are then integrated out to 0.1 cpm, the wave number where $\frac{<V_z^2>^2_{GM}}{N^2}=0.7$, to obtain $<V_z^2>$. Integrating $<V_z^2>$ out to k_c, where k_c is the cutoff wave number such that $<V_z^2>=0.7N^2$ and then taking $\frac{<V_z^2>^2}{<V_z^2>^2_{GM}}=(0.1/k_c)^2$ yielded comparable results for the most part, but often left k_c unresolved due to typical shear levels much lower than GM. Strain variance is computed by taking monthly averages of N^2 profiles as the background stratification ($\overline{N^2}$), and then computing ξ_z as $\frac{N^2-\overline{N^2}}{\overline{N^2}}$. All N^2 profiles are derived using the Fofonoff adiabatic leveling method [*Fofonoff*, 1985]. The velocity data from mooring A during 2010–2011 provided extremely high values of R_w, up to an order of magnitude higher than the results from *Kunze et al*. [2006]. We took this as an indication of instrument noise and the results have been excluded from the present analysis. A handful of similar profiles from other moorings and years with high values of R_w have been excluded as well for similar reasons. We then average the pair of profiles corresponding to the up and down MMP profiles separated by 6 h to produce daily values, at 2 day intervals. It results into 182, 173, 113, and 238 pair of profiles for moorings A, B, C, and D, respectively. Values of K_Z lower than the molecular diffusivity ($\sim 10^{-7}$ m^2 s^{-1}) are ignored in the following.

[16] The reader should keep in mind some further cautions about the applicability of the parameterization to our observations. The parameterization was initially formulated by *Gregg* [1989] for dissipation rate ε. To obtain vertical diffusivity from ε, we use the parameterization of *Osborn* [1980]: $K_Z=\gamma\varepsilon/N^2$. The mixing efficiency, γ, is taken as 0.2, following *Kunze et al*. [2006] as well as different recent studies about the Arctic Ocean [*Rainville and Winsor*, 2008; *Fer*, 2009; *Fer et al*., 2010; *Guthrie et al*., 2013]. The parameterization of *Osborn* [1980] assumes that turbulent eddies partition their energy between increasing the potential energy of the water column and dissipation through friction. This potential energy transfer requires the characterization of the density field at the eddy length scale by the buoyancy frequency, N. This requires that, in the presence of double diffusion steps as expected in the Canada Basin, the vertical resolution of the buoyancy frequency profiles should be fine enough to resolve these features. This is not the case here as, due to the limitation on available data, we apply the parameterization to profiles on a 10 m resolution grid while the staircases in this region are typically around 1 m in height [*Timmermans et al*., 2008b]. The authors acknowledge the uncertainty in applying the parameterization to a region with "stepped" stratification, however, direct comparisons of the parameterization to microstructure observations have been done in regions of the Arctic Ocean where diffusive staircases have been observed as well. *Guthrie et al*. [2013] find good agreement between the fine-scale parameterization and microstructure-derived mixing near the North Pole. In contrast, the results from the parameterization show less agreement with direct measurement in region where the salt-fingering regime has been observed, such as during the Caribbean Sheets and Layers Transects (CSALT) experiment in the Caribbean Sea [*Gregg*, 1989].

3.2. Diffusive Vertical Heat Flux

[17] Using the estimated vertical diffusivities, we compute the diffusive vertical heat flux following equation (1). Prior to the calculation, the temperature and the density profiles are interpolated to the grid on which we have obtained K_Z, and the vertical derivative of the temperature is estimated by central finite difference. The individual profiles corresponding to the up and down MMP profiles separated by 6 h are also averaged together to produce daily values (one value every 2 days).

[18] To estimate the error bars on the diffusive vertical heat flux, we assume that the uncertainty on K_Z is much larger than any other source of uncertainty. The error bars on K_Z are estimated by taking the 95% confidence limits around the integrated shear variance, V_z, given by a chi squared test, considering eight degrees of freedom (two for each component of the velocity components squared and two for the average of the up and down profiles).

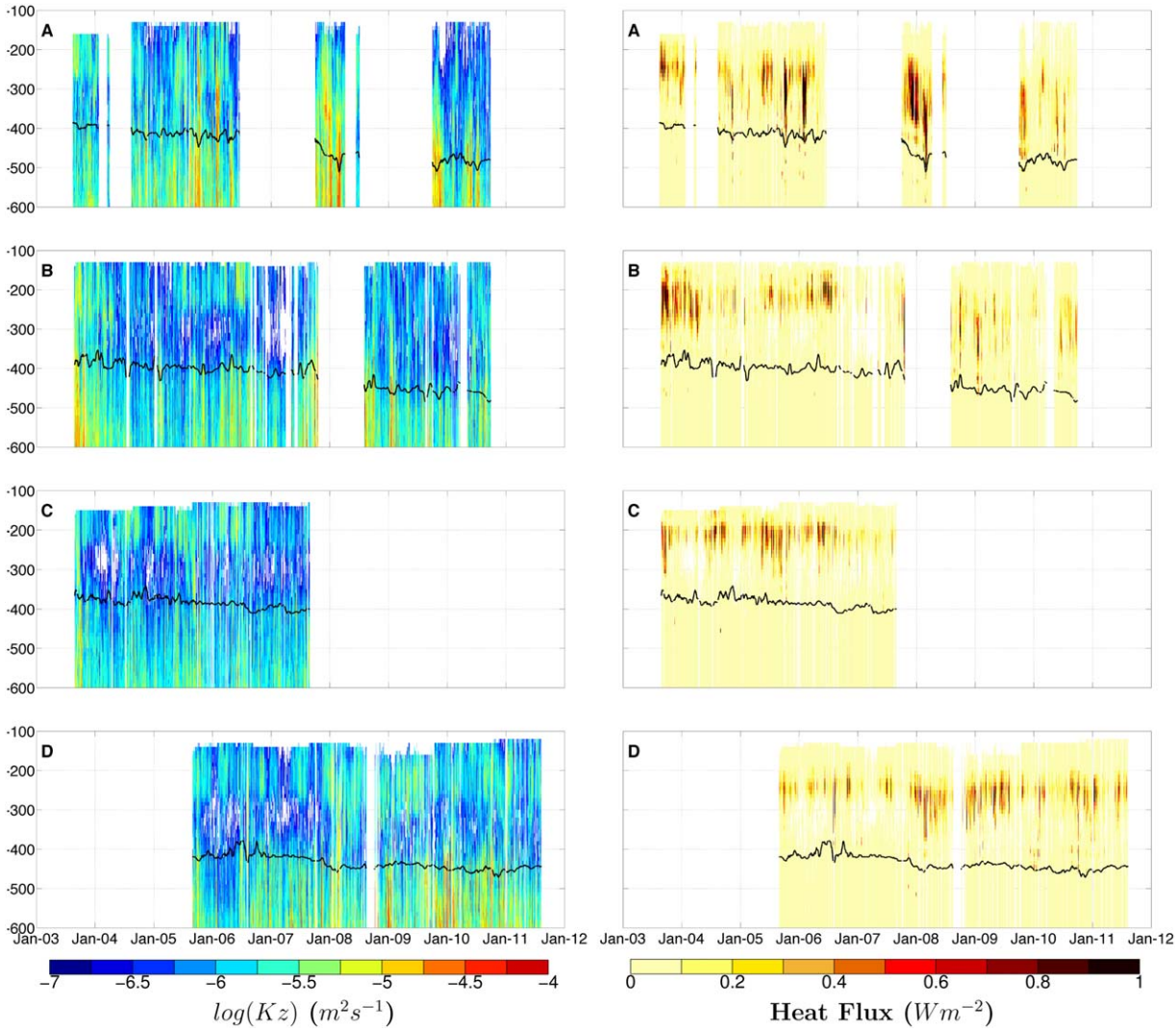

Figure 4. Vertical diffusivity and diffusive vertical heat flux as a function of time and depth for the moorings A, B, C, and D (from top to bottom). Values of K_Z lower than the molecular diffusivity (10^{-7} m^2 s^{-1}) are ignored. The black line indicates the depth of the AW temperature maximum for each mooring. Below this depth, the fine-scale parameterization is not applicable anymore due to the presence of large double diffusive intrusions.

[19] In order to assess the robustness of our results, we also compute the diffusive vertical heat flux with two constant values of K_Z: 5×10^{-6} and 10^{-6} m^2 s^{-1}. These values are high and low within the range of diffusivity values observed in the central Arctic, respectively [*Rainville and Winsor*, 2008; *Fer*, 2009].

4. Results

[20] Figure 4 shows the profile time evolution for the vertical diffusivity and the diffusive vertical heat flux for the four moorings, and the mean profiles are shown in Figure 5.

[21] In the top 450 m sampled by the four moorings, the estimated vertical diffusivity mostly varies between 3×10^{-7} and 3×10^{-5} m^2 s^{-1}, although some values reach up to 10^{-4} m^2 s^{-1}. On average, the values are low compared to diffusivity observed in the upper open ocean outside of the Arctic Basin ($\sim 10^{-5}$ m^2 s^{-1}) [e.g., *Kunze et al*., 2006], but consistent with previous estimations in the Arctic Ocean [*Rainville and Winsor*, 2008; *Fer*, 2009]. The average profile of K_Z exhibits its minimum values between 250 and 350 m ($\sim 2 \times 10^{-6}$ m^2 s^{-1}) and increases below as the stratification decreases, to reach values around to $\sim 10^{-5}$ m^2 s^{-1} at 450 m, which is the depth of the AW temperature maximum. Among the four moorings, mooring C exhibits slightly smaller K_Z values, while mooring A shows the highest mean K_Z profile. The vertical diffusivity shows large day-to-day variations, related to high variability of the energy in the velocity profiles.

[22] The resulting diffusive vertical heat flux is very close to zero, except in the transition zone between the PWW minimum temperature ($\sim$150 m) and the AW maximum temperature ($\sim$400 m), i.e., where the temperature gradient is the largest (Figure 5). At these depths, the diffusive heat flux estimated from the four moorings is $\sim$0.1–0.3 W m^{-2} on average, although it exhibits some short

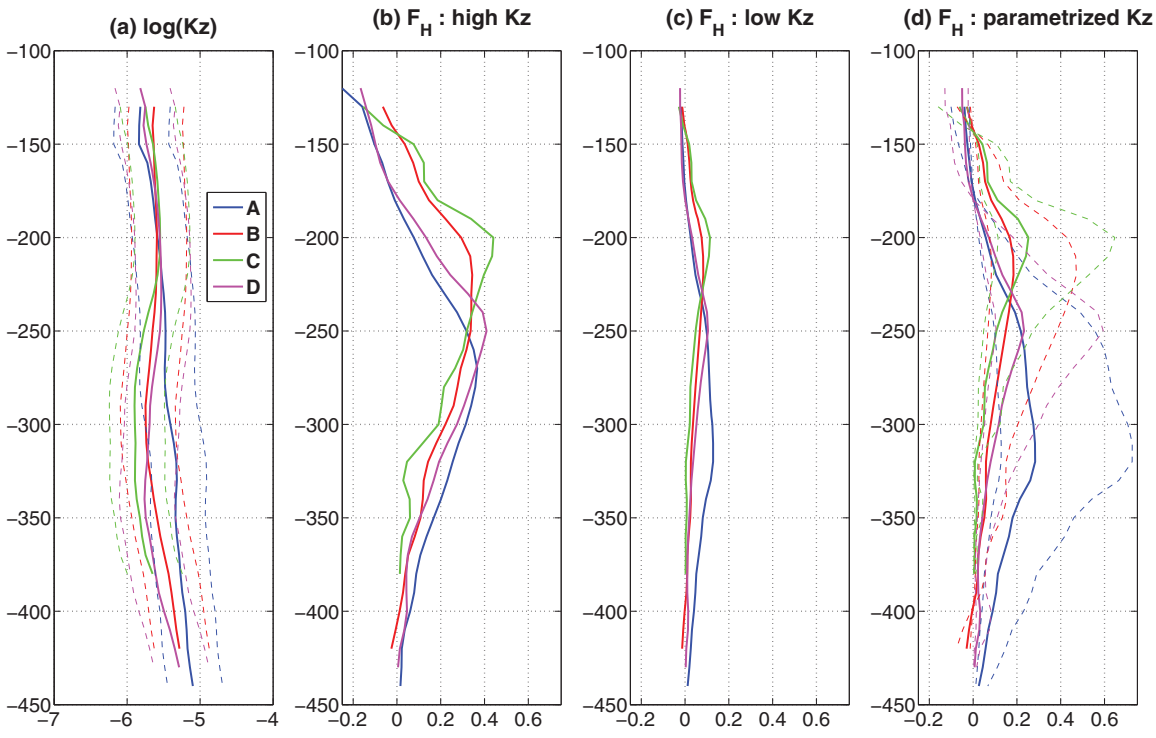

Figure 5. Time-average profiles of (a) *log* (K_Z) ($m^2\ s^{-1}$), and (b) the diffusive vertical heat flux (F_H, W m^{-2}) computed with a high constant K_Z (5.10^{-6} $m^2\ s^{-1}$), (c) a low constant K_Z (10^{-6} $m^2\ s^{-1}$), and (d) with K_Z estimated from the parameterization. The dashed lines on Figures 5a and 5d are the error bounds. The profiles are shown down to the averaged depth of the AW temperature maximum for each mooring. Below this depth, the fine-scale parameterization is not applicable anymore due to the presence of large double diffusive intrusions.

events with very high values exceeding 1 W m^{-2} (Figure 4). The maximum temperature gradient (and thus the maximum diffusive vertical heat flux computed with fixed vertical diffusivity) is found between 200 and 280 m, depending on the mooring. For the moorings B, C, and D, the time average of the diffusive vertical heat flux profile computed with the parameterized K_Z follows closely the shape of the vertical heat flux profile computed with a fixed K_Z. This shows that the vertical structure of the vertical heat flux is set by the temperature profiles at these locations. At mooring A, the diffusive vertical heat flux computed with K_Z estimated from the internal wave parameterization has its maximum deeper (~320 m) and larger (0.3 W m^{-2}) than at the other mooring locations, and also deeper than the maximum of the vertical heat flux computed with a fixed K_Z. The difference with the other moorings comes from the higher vertical diffusivity found at these depths (Figure 5a).

[23] In the following, we will investigate two sources of variability for the vertical heat flux, as we will consider the effect of (i) the temperature variations and (ii) the presence of eddies.

5. Source of Variability for the Diffusive Vertical Heat Flux

5.1. Temperature Variations

[24] In this section, we aim to examine the consequences of the AW temperature variations for the diffusive vertical heat flux between the AW and the PWW layers. To estimate the diffusive vertical heat flux from the AW layer to the overlying layer, we compute the diffusive vertical heat flux due to the temperature gradient between the AW maximum temperature (*Tmax*) and the PWW minimum temperature (*Tmin*). As discussed for instance by *McLaughlin et al*. [2009], the detection of the temperature extrema is sometimes difficult, in particular in the case of profiles containing thermal intrusions. As the temperature profiles have been interpolated to 10 m resolution for consistency with the computation of K_Z, the presence of steps tends to introduce large (and likely unrealistic) day-to-day variations of the temperature extrema and its associated depth from one profile to the other. In order to remove this effect, the temperature profiles are first smoothed (with respect to depth) with a three-point (30 m) running median smoother. The algorithm searches for the extrema values in these smoothed data, and returns the corresponding unsmoothed data value. Note that this procedure does not significantly affect the values of the temperature extrema, but rather smooths the variations of their associated depths.

[25] Once we have detected the two temperature extrema as well as their respective depth for each daily profile, we compute the diffusive vertical heat flux from the AW as:

$$F_{HAW} = \rho C_p K_Z \frac{\Delta T}{\Delta z}, \text{ with } \frac{\Delta T}{\Delta z} = \frac{Tmax - Tmin}{Z(Tmax) - Z(Tmin)} \quad (4)$$

[26] The calculation is done for a high fixed $K_Z(5\times10^{-6} m^2 s^{-1})$, and low fixed $K_Z(10^{-6}\, m^2\, s^{-1})$, and

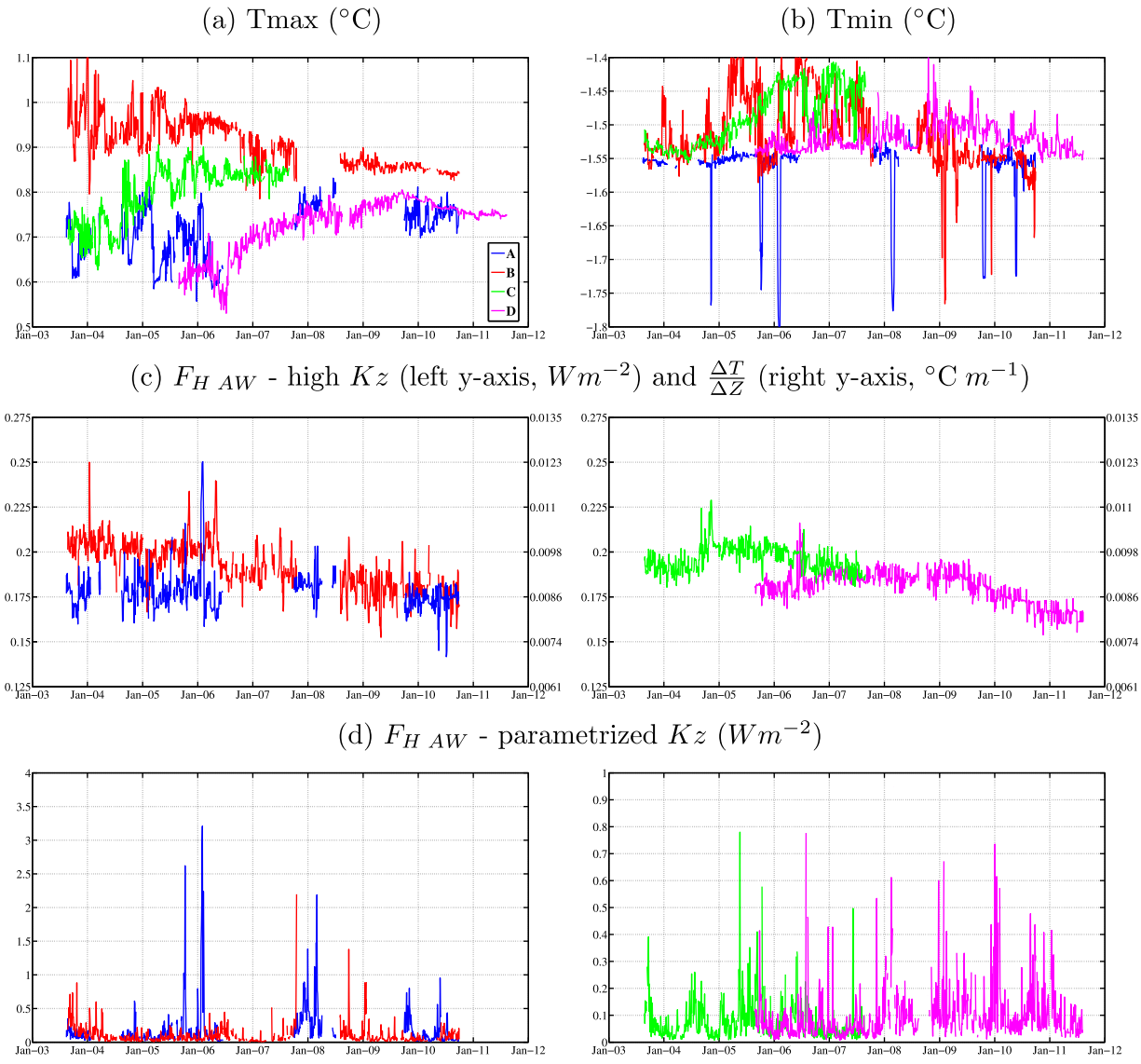

Figure 6. Time series of (a) the AW maximum temperature, (b) the PWW minimum temperature, (c) the gradient between the maximum and the minimum ($\frac{\Delta T}{\Delta Z}$, right y axis) and the diffusive vertical heat flux computed with a high K_Z (5.10^{-6} m^2 s^{-1}) (left y axis), and (d) with K_Z estimated from the parameterization averaged between the depths of the minimum and the maximum temperatures. For Figures 6c and 6d, we have separated (left) moorings A and B from (right) moorings C and D to improve readability. Note that, the scale is different for the two Figure 6d plots. For Figure 6c, the values corresponding to the vertical heat flux computed with a low K_Z (10^{-6} m^2 s^{-1}) can be obtained by divided by five the ones shown here.

K_Z estimated from the parameterization averaged between the depths of *Tmin* and *Tmax*. Results are shown in Figure 6.

[27] Overall, for the four moorings, the variations of ΔT and ΔZ are mostly driven by the variations of *Tmax* and Z(*Tmax*), respectively, as they exhibit larger amplitudes than those of *Tmin* and Z(*Tmin*) (Figure 3). This is, however, not true for a few short time periods when *Tmin* exhibits large negative anomalies due to cold anticyclonic eddies [*Timmermans et al*., 2008a], as discussed in the following part.

[28] The variations of *Tmax* at the four moorings exhibit different trends, with a large cooling affecting mooring B while moorings C and D show a warming trend. This is in agreement with the circulation scheme suggested by *McLaughlin et al*. [2009]. The large AW warming event that entered Fram Strait in the early 1990s reached mooring B (close to the Chukchi Plateau) in the late 1990s, and thus mooring B samples the cooling phase following this warm event. On the other hand, *McLaughlin et al*. [2009] shows that the warm anomaly reaches the interior of the Canada Basin through the spreading of thermohaline intrusions by an anticyclonic flow. Thus, the AW warm anomaly reaches mooring C (showing a *Tmax* warming trend over 2004–2006) and then mooring D (warming trend over 2006–2008). After the warming trend, *Tmax* at moorings C and D

Table 1. Mean and Standard Deviations of the Diffusive Vertical Heat Flux Between the AW Maximum Temperature and the PWW Minimum Temperature, Computed With a High K_Z (10^{-5} m^2 s^{-1}) and With K_Z Estimated From the Parameterization Averaged Between the Depths of the Minimum and the Maximum Temperatures

	$F_{H\,AW}$ − High K_Z (W m^{-2})		$F_{H\,AW}$ − Parameterized KZ (W m^{-2})	
	Mean	Std	Mean	Std
Mooring A	0.18	0.01	0.19	0.3
Mooring B	0.19	0.01	0.13	0.1
Mooring C	0.20	0.007	0.07	0.07
Mooring D	0.18	0.01	0.09	0.12

is roughly constant. As noted by *McLaughlin et al*. [2009], the AW temperature at mooring A is mostly driven by year-to-year variations rather than trend, likely due to the multiple spreading pathways of the warm anomaly over and around the Chukchi Plateau and into the interior, that may have reached the location of mooring A at different times.

[29] At the four moorings, the depths of *Tmax* and *Tmin* deepen with time (Figure 3), with a clear trend starting in 2006. The downward trend affects all isotherms, in a coherent way over the whole water column, although the deepening of the AW layer is greater than the deepening of the PWW layer. The strongest trend affects moorings A and B, where *Tmax* deepens by ∼80 m between 2003 and 2010 while *Tmin* deepens by ∼50−60 m. Over the same period, *Proshutinsky et al*. [2009] observed an intensification of Beaufort Gyre in the Canada Basin, due to the enhanced Arctic high anticyclonic circulation over the region. The deepening of the isotherms is likely related to the downwelling associated with the Ekman pumping increase in the Basin [*Yang*, 2006]. Based on chemical and optical data, *Jackson et al*. [2010] and *McLaughlin and Carmack* [2010] have reported a similar deepening of the nutricline and chlorophyll maximum in the interior of the Canada Basin over the period 2003–2009. The more rapid deepening of the *Tmax* isotherm relative to the *Tmin* isotherm also suggests a thickening of the intermediate layer of the water column after 2006.

[30] Mean values and standard deviations of $F_{H\,AW}$ computed with both a fixed K_Z and a parameterized K_Z for the different moorings are indicated in Table 1. When using a fixed value of vertical diffusion, the mean values of $F_{H\,AW}$ at the four moorings are almost equal (∼0.2 W m^{-2} for a K_Z value of 5×10^{-6} m^2 s^{-1}). The standard deviation remains small for the four moorings (0.01 W m^{-2}), and $F_{H\,AW}$ mostly exhibits low-frequency variability (Figure 6c). After 2006, $F_{H\,AW}$ exhibits a decreasing trend at the four moorings, with similar low-frequency variability among the different locations. This is due to the difference in the trends of the *Tmax* and *Tmin* depths, which drives most of the variations and trend of $\frac{\Delta T}{\Delta Z}$ after 2006, and in turn of the heat flux evolution computed with a fixed vertical diffusion value. During the early years of the time series, the depth of the temperature maximum remains roughly constant and the variations of the heat flux computed with a fixed value of vertical diffusion for the four moorings closely follows the shape of the *Tmax* time series.

[31] $F_{H\,AW}$ computed with the vertical diffusivity estimated from the parameterization shows a very different behavior than $F_{H\,AW}$ computed with a constant vertical diffusivity (Figure 6d). For the four moorings, the time series exhibit low background values (∼0.05 W m^{-2}) on which strong events (∼1 or 2 days) are superimposed. These events explain the mean values of $F_{H\,AW}$ higher than the "background values," as well as the large standard deviations shown in Table 1. The four moorings are affected by events with strong diffusive heat flux, although the maximum value of $F_{H\,AW}$ during these events remains much smaller at C and D than at A and B (Figure 6d). Most of these events are due to the presence of eddies that tend to increase the vertical diffusivity through a change of both the buoyancy frequency and the velocity profiles. This will be investigated in the following part.

[32] Does the upward diffusive heat flux from the AW affect the overlying PWW layer temperature? We could not find a significant statistical relationship between the time series of the PWW temperature and $F_{H\,AW}$ at any of the four mooring locations. This is likely because the vertical diffusion is overshadowed by horizontal advection of heat in the PWW layer.

5.2. Eddies

[33] *Timmermans et al*. [2008a] provide a review of the characteristics of the eddies observed in the Canada Basin, most of which are cold core anticyclonic eddies. They report that eddies have different properties, depending on their location in the Canada Basin. At moorings A and B, the PWW temperature exhibits some strong events when *Tmin* decreases by ∼0.2°C during a few days (Figure 6b). These are the signature of subsurface eddies, as revealed by the time-depth evolution of the buoyancy frequency (Figure 3), where strong negative anomalies can be seen between 150 and 300 m but does not extend to the upper layer and the surface. This is consistent with the findings of *Manley and Hunkins* [1985], who have observed numerous subsurface eddies in the region of moorings A and B, with a diameter of 10–20 km, and confined in depth between 50 and 300 m. They found that these eddies have a cold core signature, with an anomaly of ∼0.2°C in the center of the eddies, which is similar to the cold anomalies affecting the PWW minimum temperature during these events (Figure 6b). Eddies with similar temperature and salinity characteristics have also been observed close to the locations of these two moorings by *Newton et al*. [1974], *D'Asaro* [1988], and *Padman et al*. [1990].

[34] On the other hand, the locations of moorings C and D are closer to the studied area of *Timmermans et al*. [2008a], where they observed shallower eddies (with center depths between 40 and 70 m). The buoyancy frequency at these moorings (Figure 3) does not show events with large negative anomalies below ∼150 m (i.e., the shallowest depth where the computation of the vertical diffusivity can be done). An examination of the buoyancy frequency above these depths (not shown) suggest the presence of such eddies, although they are not fully resolved. However, these eddies are too shallow to directly affect the diffusive

heat flux from the AW layer, although they may have a significant impact for the transfer of heat from the Pacific layer to the cold halocline. Observations of the upper layer of the water column would be required to quantify this effect.

[35] Does the presence of subsurface eddies affect the diffusive vertical heat flux from the AW layer? When mooring A or B samples a subsurface eddy, the minimum temperature of the profile decreases by ∼0.2°C for a day or two. Considering a constant high K_Z and no change of *Tmax* and the depths of *Tmax* and *Tmin*, this would correspond to an increase of $F_{H\,AW}$ by 0.02 W m^{-2}. This represents about 10% of the mean values.

[36] Figure 6d shows a much larger increase in the presence of eddies (up to 3 W m^{-2} for mooring A), owing to the large increase of the vertical diffusivity. This increase of the vertical diffusivity might be however overestimated by our calculation method and the values obtained here have to be taken with caution. There are observational and theoretical aspects to our caution, as the coupling among eddies, internal waves, and mixing is poorly understood [*Perkins*, 1976; *Polzin*, 2008]. In fact, our use of the fine-scale parameterization relies on the idea that the disturbances of the velocity and buoyancy frequency from their averages are due to internal waves, which is not solely true in the presence of eddy-derived shear and strain. For this paper, we have not derived a method of separating internal wave and eddy-derived disturbances in our measurements. Further, we are uncertain about the applicability of the assumptions underlying internal wave parameterization of mixing inside eddies. The internal wave energy displayed at one location is ultimately dissipated at another location. If the internal wavefield is horizontally homogeneous this will not matter when applying the parameterization, but particularly in the typically small Arctic eddies, the internal wave energy dissipation at one location may be much higher or lower than would be indicated by the local internal wave energy itself.

[37] With these cautions in mind, we infer that the change of the K_Z value in the presence of eddy results from an interplay between the change of stratification (Figure 3) and the change in the velocity profile, with speeds that can reach up to ∼15 cm s^{-1} (Figure 7 for mooring A). Depending if the mooring samples the core or the edge of the subsurface eddies, the signature of the eddies might be stronger in the stratification or the velocity profiles. Our calculations suggest that subsurface eddies are responsible for some enhanced diffusive vertical heat flux, mostly in the region of moorings A and B, although, the increase of the resulting vertical heat flux only lasts 1 or 2 days (Figure 6). More investigation would be required to properly quantify the efficiency of the transfer of heat from the AW layer to the Pacific water layer in the presence of eddies, as the moorings only detect a few eddies over the decade of observations (Figure 3).

6. Conclusion and Discussion

[38] Mooring observations were used to quantify the diffusive vertical heat flux, with emphasis on the amount of heat released upward from the AW layer lying at intermediate depth in the Arctic Ocean. Almost a decade (2003–2011) of MMP profiles taken at four different locations in the Canada Basin were analyzed in this regard. The vertical diffusivity is estimated using a parameterization accounting for energy dissipation by internal waves breaking, following *Kunze et al*. [2006]. This provides for the first time (to our knowledge) a time series of vertical diffusivity profiles in the Arctic Basin.

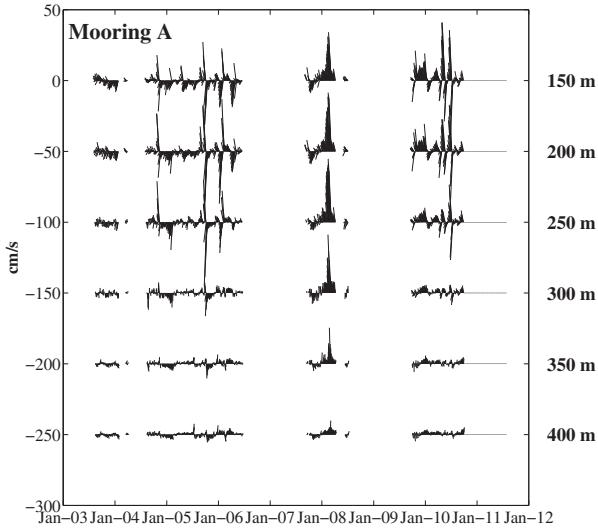

Figure 7. Stick diagram of currents at six depths for mooring A. Successive depths are offset by −50 cm s^{-1}.

[39] The computation yields diffusive vertical heat fluxes between 0.1 and 0.2 W m^{-2} on average, depending on the location of the mooring. This is only a small fraction of the 6.7 W m^{-2} required to maintain a steady state for the AW layer [*Turner*, 2010], but the diffusive heat flux is of the same order of magnitude as the heat flux due to double diffusion estimated in the interior of the Canada Basin (between 0.05 and 0.3 W m^{-2}) [*Timmermans et al*., 2008b]. When computed independently, the sum of the diffusive contribution and the double diffusion contribution to the vertical heat flux represents an upper limit of the real vertical heat flux [*Inoue et al*., 2007]. This suggests that the upward transfer of heat from the AW layer in the central Canadian Basin accounts only for a small fraction of the total transfer. From hydrography, we know that the bulk of the heat flux from the AW occurs north and east of Fram Strait in the Nansen Basin [*Treshnikov*, 1977], most likely during winter mixed layer convection, and further downstream in the basin in "hot spots" on the slope due to enhanced mixing [*Padman and Dillon*, 1991]. The small contribution of the heat flux in the interior of the Canada Basin suggest that other mechanisms need to be at play to close the large-scale budget, and should be examined with more attention in order to quantify their contribution. Among them, recent observations or modeling studies point out the possible importance of double diffusion on the slope in the Laptev Sea [*Polyakov et al*., 2012], brine convection originated from sea ice leads that can reach the base of the mixed layer [*Matsumura and Hasumi*, 2008] or ice band formation and the associated vertical velocity that could propagate up to the AW layer [*Fujisaki and Oey*, 2011].

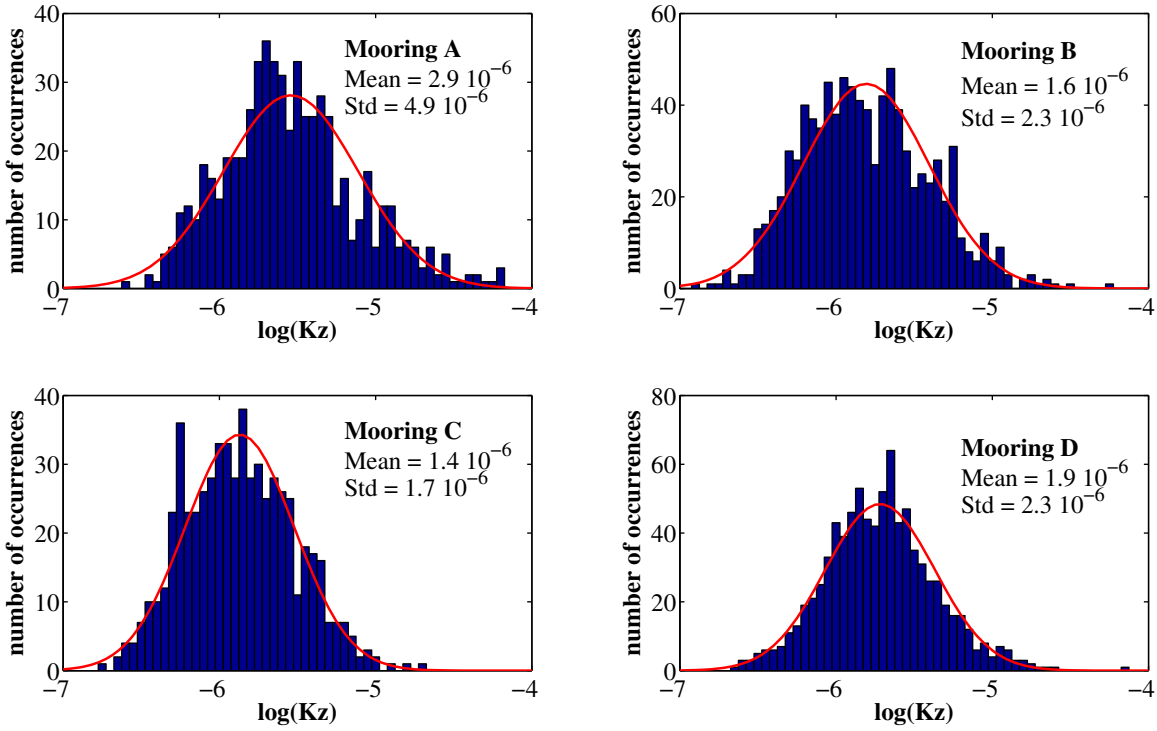

Figure 8. Histogram of the distribution (in number of occurrences) of K_Z (in $m^2\ s^{-1}$) estimated from the parameterization averaged between the depths of the minimum and the maximum temperatures. The best Gaussian fit is indicated in red. Means and standard deviations of the distribution are also indicated for each mooring.

[40] We also examined the variability of the diffusive vertical heat flux between the AW layer and the PWW layer. Although the AW temperature exhibits large variations between 2003 and 2011 [*McLaughlin et al*., 2009], it yields small variations for the temperature gradient (which is mostly controlled by the depth of the AW temperature maximum) and thus the diffusive vertical heat flux.

[41] One of the mooring samples several strong cold anticyclonic eddies just above the AW layer. Their passage affects the stratification and the velocity profiles, leading to higher vertical diffusivity, although more investigation is required to quantify their effect properly. We speculate that eddies could be an efficient mechanism to transfer heat to the overlying layer in the interior of the Canada Basin. However, only one out of the four moorings sample eddies lying on top of the AW layer and thus susceptible to enhance the diffusive vertical heat flux, suggesting that this mechanism for upward transfer of heat, although possibly efficient, remains limited and intermittent both in time and space.

[42] Due to the very few number of estimates of the vertical diffusivity in the Arctic interior and in particular in the Canadian Basin, some authors have estimated the heat vertical diffusion using constant values for the vertical diffusivity [e.g., *Jackson et al*., 2011]. One could, however, question this approximation, as we found that K_Z varies strongly in time (Figure 4). The distribution of the vertical diffusivity at the four moorings is shown in Figure 8. The results suggest that computing diffusive vertical heat flux in the interior of the Canada Basin with a constant vertical diffusivity ($\sim 2 \times 10^{-6}\ m^2\ s^{-1}$) provides a reasonable estimate of the upward heat transfer from the AW layer. The distribution for mooring A (where eddies are mostly sampled) presents however a larger standard deviation, suggesting that the approximation of a constant diffusivity breaks down in the presence of eddies, as they might strongly affect the vertical diffusivity and in turn the upward diffusive heat flux. The choice of a correct background diapycnal diffusivity value appears to be crucial in numerical models to properly simulate many aspect of the Arctic dynamics, including the stratification and the AW circulation [*Zhang and Steele*, 2007]. The optimal value used in the Pan-Arctic Ice Ocean Modeling and Assimilation System (PIOMAS) model ($\sim 2 \times 10^{-6}\ m^2\ s^{-1}$) (J. Zhang, personal communication, 2013) agrees with our average value in the Canada Basin.

[43] **Acknowledgments.** C. Lique acknowledge support from JISAO and the Program on Climate Change of the University of Washington. J. Guthrie and J. Morison are supported by National Science Foundation grants ARC-0909408 and ARC-0856330. M. Steele is supported by the Office of Naval Researches Arctic and Global Prediction Program, by NSFs Division of Polar Programs, and by NASAs Cryosphere and Physical Oceanography programs. The MMP data were collected and made available by the Beaufort Gyre Exploration Program based at the Woods Hole Oceanographic Institution (http://www.whoi.edu/beaufortgyre) in collaboration with researchers from Fisheries and Oceans Canada at the Institute of Ocean Sciences. Support for the BGOS program and R. Krishfield was provided by the National Science Foundation (under grants ARC-0806115, ARC-0631951, ARC-0806306, and ARC-0856531) and Woods Hole Oceanographic Institution internal funding. For A. Proshutinsky, this research is supported by the National Science Foundation Office of Polar Programs, awards ARC-1203720 and ARC-0856531.

References

Aagaard, K., L. Coachman, and E. Carmack (1981), On the halocline of the Arctic Ocean, *Deep Sea Res., Part A*, *28*, 529–545, doi:10.1016/0198-0149(81)90115-1.

Carmack, E. C., R. W. Macdonald, R. G. Perkin, F. A. McLaughlin, and R. J. Pearson (1995), Evidence for warming of Atlantic Water in the Southern Canadian Basin of the Arctic Ocean: Results from the Larsen-93 expedition, *Geophys. Res. Lett.*, *22*, 1061–1064, doi:10.1029/95GL00808.

Carmack, E. C., K. Aagaard, J. H. Swift, R. W. MacDonald, F. A. McLaughlin, E. Peter Jones, R. G. Perkin, J. N. Smith, K. M. Ellis, and L. R. Killius (1997), Changes in temperature and tracer distributions within the Arctic Ocean: Results from the 1994 Arctic Ocean section, *Deep Sea Res., Part II*, *44*, 1487–1502, doi:10.1016/S0967-0645(97)00056-8.

Carpenter, J. R., and M.-L. Timmermans (2012), Deep mesoscale eddies in the Canada Basin, Arctic Ocean, *Geophys. Res. Lett.*, *39*, L20602, doi:10.1029/2012GL053025.

Coachman, L. K., and C. A. Barnes (1961), The contribution of Bering Sea water to the Arctic Ocean, *Arctic*, *14*, 147–161.

D'Asaro, E., and J. Morison (1992), Internal waves and mixing in the Arctic Ocean, *Deep Sea Res., Part A*, *39*, 459–484, doi:10.1016/S0198-0149(06)80016-6.

D'Asaro, E. A. (1988), Observations of small eddies in the Beaufort Sea, *J. Geophys. Res.*, *93*, 6669–6684, doi:10.1029/JC093iC06p06669.

D'Asaro, E. A., and M. D. Morehead (1991), Internal waves and velocity fine structure in the Arctic Ocean, *J. Geophys. Res.*, *96*, 12,725–12,738, doi:10.1029/91JC01071.

Fer, I. (2009), Weak vertical diffusion allows maintenance of cold halocline in the central Arctic, *Atmos. Oceanic Sci. Lett.*, *2*(3), 148–152.

Fer, I., R. Skogseth, and F. Geyer (2010), Internal waves and mixing in the marginal ice zone near the Yermak Plateau*, *J. Phys. Oceanogr.*, *40*, 1613–1630, doi:10.1175/2010JPO4371.1.

Fofonoff, N. P. (1985), Physical properties of seawater: A new salinity scale and equation of state for seawater, *J. Geophys. Res.*, *90*, 3332–3342, doi:10.1029/JC090iC02p03332.

Fujisaki, A., and L.-Y. Oey (2011), Formation of ice bands by winds, *J. Geophys. Res.*, *116*, C10015, doi:10.1029/2010JC006655.

Gregg, M. C. (1989), Scaling turbulent dissipation in the thermocline, *J. Geophys. Res.*, *94*, 9686–9698, doi:10.1029/JC094iC07p09686.

Gregg, M. C., T. B. Sanford, and D. P. Winkel (2003), Reduced mixing from the breaking of internal waves in equatorial waters, *Nature*, *422*, 513–515, doi:10.1038/nature01507.

Guthrie, J. D., J. H. Morison, and I. Fer (2013), Revisiting internal waves and mixing in the Arctic Ocean, *J. Geophys. Res.*, *118*, 3966–3977, doi:10.1002/jgrc.20294.

Inoue, R., H. Yamazaki, F. Wolk, T. Kono, and J. Yoshida (2007), An estimation of buoyancy flux for a mixture of turbulence and double diffusion, *J. Phys. Oceanogr.*, *37*, 611–624, doi:10.1175/JPO2996.1.

Jackson, J. M., S. E. Allen, E. C. Carmack, and F. A. McLaughlin (2010), Suspended particles in the Canada Basin from optical and bottle data, 2003–2008, *Ocean Sci.*, *6*, 799–813, doi:10.5194/os-6-799-2010.

Jackson, J. M., S. E. Allen, F. A. McLaughlin, R. A. Woodgate, and E. C. Carmack (2011), Changes to the near-surface waters in the Canada Basin, Arctic Ocean from 1993–2009: A basin in transition, *J. Geophys. Res.*, *116*, C10008, doi:10.1029/2011JC007069.

Kunze, E., E. Firing, J. M. Hummon, T. K. Chereskin, and A. M. Thurnherr (2006), Global abyssal mixing inferred from lowered ADCP shear and CTD strain profiles, *J. Phys. Oceanogr.*, *36*, 1553–1576, doi:10.1175/JPO2926.1.

Manley, T. O., and K. Hunkins (1985), Mesoscale eddies of the Arctic Ocean, *J. Geophys. Res.*, *90*, 4911–4930, doi:10.1029/JC090iC03p04911.

Matsumura, Y., and H. Hasumi (2008), Brine-driven eddies under sea ice leads and their impact on the Arctic Ocean mixed layer, *J. Phys. Oceanogr.*, *38*, 146–163, doi:10.1175/2007JPO3620.1.

McLaughlin, F. A., and E. C. Carmack (2010), Deepening of the nutricline and chlorophyll maximum in the Canada Basin interior, 2003–2009, *Geophys. Res. Lett.*, *37*, L24602, doi:10.1029/2010GL045459.

McLaughlin, F. A., E. C. Carmack, W. J. Williams, S. Zimmermann, K. Shimada, and M. Itoh (2009), Joint effects of boundary currents and thermohaline intrusions on the warming of Atlantic Water in the Canada Basin, 1993–2007, *J. Geophys. Res.*, *114*, C00A12, doi:10.1029/2008JC005001.

Merryfield, W. J. (2000), Origin of thermohaline staircases, *J. Phys. Oceanogr.*, *30*, 1046–1068, doi:10.1175/1520-0485(2000)030<1046:OOTS>2.0.CO;2.

Morison, J., M. Steele, and R. Andersen (1998), Hydrography of the upper Arctic Ocean measured from the nuclear submarine U.S.S. Pargo, *Deep Sea Res., Part I*, *45*, 15–38, doi:10.1016/S0967-0637(97)00025-3.

Newton, J., K. Aagaard, and L. Coachman (1974), Baroclinic eddies in the Arctic Ocean, *Deep Sea Res. Oceanogr. Abstr.*, *21*(9), 707–719.

Osborn, T. R. (1980), Estimates of the local rate of vertical diffusion from dissipation measurements, *J. Phys. Oceanogr.*, *10*, 83–89, doi:10.1175/1520-0485(1980)010<0083:EOTLRO>2.0.CO;2.

Padman, L., and T. M. Dillon (1987), Vertical heat fluxes through the Beaufort Sea Thermohaline staircase, *J. Geophys. Res.*, *92*, 10,799–10,806, doi:10.1029/JC092iC10p10799.

Padman, L., and T. M. Dillon (1988), On the horizontal extent of the Canada Basin thermohaline steps, *J. Phys. Oceanogr.*, *18*, 1458–1464, doi:10.1175/1520-0485(1988)018<1458:OTHEOT>2.0.CO;2.

Padman, L., and T. M. Dillon (1989), Thermal microstructure and internal waves in the Canada Basin diffusive staircase, *Deep Sea Res., Part A*, *36*, 531–542.

Padman, L., and T. M. Dillon (1991), Turbulent mixing near the Yermak Plateau during the coordinated Eastern Arctic experiment, *J. Geophys. Res.*, *96*, 4769–4782, doi:10.1029/90JC02260.

Padman, L., M. Levine, T. Dillon, J. Morison, and R. Pinkel (1990), Hydrography and microstructure of an Arctic cyclonic eddy, *J. Geophys. Res.*, *95*, 9411–9420, doi:10.1029/JC095iC06p09411.

Perkins, H. (1976), Observed effect of an eddy on inertial oscillations, *Deep Sea Res. Oceanogr. Abstr.*, *23*, 1037–1042.

Polyakov, I. V., G. V. Alekseev, L. A. Timokhov, U. S. Bhatt, R. L. Colony, H. L. Simmons, D. Walsh, J. E. Walsh, and V. F. Zakharov (2004), Variability of the intermediate Atlantic Water of the Arctic Ocean over the last 100 years, *J. Clim.*, *17*, 4485–4497, doi:10.1175/JCLI-3224.1.

Polyakov, I. V., et al. (2010), Arctic Ocean warming contributes to reduced polar ice cap, *J. Phys. Oceanogr.*, *40*, 2743–2756, doi:10.1175/2010JPO4339.1.

Polyakov, I. V., A. V. Pnyushkov, R. Rember, V. V. Ivanov, Y.-D. Lenn, L. Padman, and E. C. Carmack (2012), Mooring-based observations of double-diffusive staircases over the Laptev Sea slope, *J. Phys. Oceanogr.*, *42*, 95–109, doi:10.1175/2011JPO4606.1.

Polzin, K. L. (2008), Mesoscale eddy-internal wave coupling. Part I: Symmetry, wave capture, and results from the mid-ocean dynamics experiment, *J. Phys. Oceanogr.*, *38*, 2556–2574, doi:10.1175/2008JPO3666.1.

Polzin, K. L., J. M. Toole, J. R. Ledwell, and S. R. W. (1997), Spatial variability of turbulent mixing in the Abyssal Ocean, *Science*, *276*(5309), 93–96.

Proshutinsky, A., R. Krishfield, M.-L. Timmermans, J. Toole, E. Carmack, F. McLaughlin, W. J. Williams, S. Zimmermann, M. Itoh, and K. Shimada (2009), Beaufort Gyre freshwater reservoir: State and variability from observations, *J. Geophys. Res.*, *114*, C00A10, doi:10.1029/2008JC005104.

Quadfasel, D., A. Sy, D. Wells, and A. Tunik (1991), Warming in the Arctic, *Nature*, *350*, 385, doi:10.1038/350385a0.

Rainville, L., and P. Winsor (2008), Mixing across the Arctic Ocean: Microstructure observations during the Beringia 2005 Expedition, *Geophys. Res. Lett.*, *35*, L08606, doi:10.1029/2008GL033532.

Rudels, B., L. G. Anderson, and E. P. Jones (1996), Formation and evolution of the surface mixed layer and halocline of the Arctic Ocean, *J. Geophys. Res.*, *101*, 8807–8822, doi:10.1029/96JC00143.

Shimada, K., F. McLaughlin, E. Carmack, A. Proshutinsky, S. Nishino, and M. Itoh (2004), Penetration of the 1990s warm temperature anomaly of Atlantic Water in the Canada Basin, *Geophys. Res. Lett.*, *31*, L20301, doi:10.1029/2004GL020860.

Shimada, K., M. Itoh, S. Nishino, F. McLaughlin, E. Carmack, and A. Proshutinsky (2005), Halocline structure in the Canada Basin of the Arctic Ocean, *Geophys. Res. Lett.*, *32*, L03605, doi:10.1029/2004GL021358.

Sirevaag, A., and I. Fer (2012), Vertical heat transfer in the Arctic Ocean: The role of double-diffusive mixing, *J. Geophys. Res.*, *117*, C07010, doi:10.1029/2012JC007910.

Smethie, W. M., P. Schlosser, G. Bönisch, and T. S. Hopkins (2000), Renewal and circulation of intermediate waters in the Canadian Basin observed on the SCICEX 96 cruise, *J. Geophys. Res.*, *105*, 1105–1121.

Steele, M., and J. H. Morison (1993), Hydrography and vertical fluxes of heat and salt northeast of Svalbard in autumn, *J. Geophys. Res.*, *98*, 10,013–10,024, doi:10.1029/93JC00937.

Steele, M., J. Morison, W. Ermold, I. Rigor, M. Ortmeyer, and K. Shimada (2004), Circulation of summer Pacific halocline water in the Arctic Ocean, *J. Geophys. Res.*, *109*, C02027, doi:10.1029/2003JC002009.

Timmermans, M.-L., J. Toole, A. Proshutinsky, R. Krishfield, and A. Plueddemann (2008a), Eddies in the Canada Basin, Arctic Ocean, observed from ice-tethered profilers, *J. Phys. Oceanogr.*, *38*, 133–145, doi:10.1175/2007JPO3782.1.

Timmermans, M.-L., J. Toole, R. Krishfield, and P. Winsor (2008b), Ice-tethered profiler observations of the double-diffusive staircase in the Canada Basin thermocline, *J. Geophys. Res.*, *113*, C00A02, doi:10.1029/2008JC004829.

Toole, J. M., M.-L. Timmermans, D. K. Perovich, R. A. Krishfield, A. Proshutinsky, and J. A. Richter-Menge (2010), Influences of the ocean surface mixed layer and thermohaline stratification on Arctic Sea ice in the central Canada Basin, *J. Geophys. Res.*, *115*, C10018, doi:10.1029/2009JC005660.

Treshnikov, A. (1977), Water masses of the Arctic Ocean, in *Polar Oceans*, edited by M. Dunbar, pp. 17–31, Arctic Inst. of N. Am., Calgary, Canada.

Turner, J. S. (2010), The melting of ice in the Arctic Ocean: The influence of double-diffusive transport of heat from below, *J. Phys. Oceanogr.*, *40*, 249–256, doi:10.1175/2009JPO4279.1.

Yang, J. (2006), The seasonal variability of the Arctic Ocean Ekman transport and its role in the mixed layer heat and salt fluxes, *J. Clim.*, *19*, 5366–5387, doi:10.1175/JCLI3892.1.

Zhang, J., and M. Steele (2007), Effect of vertical mixing on the Atlantic Water layer circulation in the Arctic Ocean, *J. Geophys. Res.*, *112*, C04S04, doi:10.1029/2006JC003732.